ELSEVIER

Growth and characterization of Sm^{3+}-substituted PZT thin films

S.K. Pandey[a], Shiv Kumar[a], S.N. Chatterjee[a], Upendra Kumar[a],
Chandra Prakash[a,*], Ratnamala Chatterjee[b], T.C. Goel[c]

[a]*Electroceramics Group, Solid State Physics Laboratory, Lucknow Road, Delhi-110 054, India*
[b]*Department of Physics, Indian Institute of Technology, New Delhi-110 016, India*
[c]*Birla Institute of Technology and Science, Goa-403726, India*

Abstract

We report a systematic study on growth of 2% and 4% Samarium (Sm) substituted lead zirconate titanate (PZT) thin films (with molar ratio of Zr:Ti::65/35) by sol gel technique on Pt/Si $\langle 1\,0\,0 \rangle$ and Pt/Si $\langle 1\,1\,1 \rangle$ substrates. XRD analysis show single phase for all films. Surface morphology was studied using atomic force microscope (AFM). A metal/ferroelectric/metal (MFM) structure was formed by depositing gold electrode on top of the film for electrical measurements (I–V (current vs voltage), C–V (capacitance vs voltage), P–E (polarization vs electric field)). The films show well-defined ferroelectric behaviour for both compositions (2% and 4% Sm-substituted PZT). I–V measurements show a compositional shift along −ve (negative) voltage axis. To obtain optical band gap, films were deposited on fused quartz and transmittance measurements were performed. Optical band gap was calculated from $(\alpha h \upsilon)^2$ vs $h\upsilon$ graph (where α is the extinction coefficient, h the planck's constant and υ the frequency of light). The results are discussed.

1. Introduction

Lead zirconate titanate (PZT) ceramics (bulk and thin films) with various substituents have been studied in the past and the studies have been compiled by Heartling [1]. Among the substituents, Sm (Samarium) has attracted the attention of researchers due to its comparable ionic radii (~0.96 Å) with reference to lead (Pb~1.19 Å). The effect of Sm modification on PZT (65/35) ceramics showing high pyroelectric coefficient has been studied [2]. Samarium has also been substituted in other PbTiO$_3$ and PZT-based ceramics [3–5]. Further the effect of rare-earth ions on the microstructural and electrical properties of PZT ceramics has been reported by Shanigrahi et al. [6].

In selecting appropriate trivalent cationic species for ferroelectric applications, one has to consider various physicochemical factors. Among these, the following three factors seem to be most appropriate: (i) stability of perovskite phase; (ii) ionic radius; and (iii) Curie–Weiss temperature [7]. Among trivalent lanthanides, samarium Sm seems to satisfy all the three criteria for its substitution in PZT. Its ionic radius of ~0.96 Å is suitable enough to substitute Pb on A-site. The Curie–Weiss temperature of PbSmZT has been reported as ~150 °C [2], which is high enough to be used in ferroelectric memory devices that require a stability of polarization switching against thermal agitation. It may also be noted that addition or substitution of foreign ions (Sm^{3+}) in perovskite structures may normally affect: (a) transition temperature; (b) compositional homogeneity; (c) domain wall motion; (d) valence state of other additives; (e) vacancy distribution at A, B and O-sites; (f) oxygen contents and (g) valency of Ti or Zr atoms. Properties like Curie temperature,

---

*Corresponding author. Tel.: +91 11 2392 1692; fax: +91 11 2391 3609.
E-mail addresses: 628@ssplnet.org (S.K. Pandey), c_prakash@vsnl.net (C. Prakash).

dielectric constant and loss (tan δ), etc. of PZT ceramics can be improved by modifying them with small amount of samarium. Sm^{3+} ions substitute for Pb^{2+} ions and a defect due to Sm is compensated for the electrons in the conduction band derived from 3-d state of Ti or Zr atom. As charge on Sm is higher than that of Pb, it acts as a donor, however, if charge on the modifier ions is less than the one it replaces, then it acts as acceptor. In a chemical equation, charge electro-neutrality must be maintained and all available sites must be filled but sometimes non-isovalent substitutions are made intentionally.

A variety of techniques have been proposed to fabricate PZT films, such as metallorganic chemical vapour deposition (MOCVD), sputtering, sol–gel, PLD, etc. Among them sol–gel method is one of the most popular choices because of its better solution homogeneity, ease of tailoring the compositions and scalability/large area deposition.

In this article, we report a systematic study on the structural, electrical and optical properties of Pb_{1-x} $Sm_x(Zr_{0.65}Ti_{0.35})O_3$ ($x = 0.02, 0.04$) films (hereafter PSZT).

2. Experimental details

PSZT thin films were prepared by sol–gel technique using lead acetate tri-hydrate, samarium(III) acetate tri-hydrate, zirconium-acetyl-acetonate, and titanium-iso-propoxide as precursors. 2-Methoxy-ethanol and acetic acid were used as solvents. A 4% excess of the lead precursor was added to the solution to compensate for the deficiency in lead concentration and to assist crystallization. $Pt/TiO_2/SiO_2/Si \langle 1 0 0 \rangle$, $Pt/TiO_2/SiO_2/Si \langle 1 1 1 \rangle$ and fused quartz were used as substrates. Seed layers of $PbTiO_3$ (PT) prepared by sol–gel technique using the above-mentioned alkoxides ($\sim 0.1 \mu m$ thickness) were deposited on the substrates before depositing PSZT layers. A spin coating unit (Model PRS-4000) was used for the deposition of all sol–gel films. Substrates held by a vacuum-chuck were rotated at speeds of 2000 rpm for 20 s at each and every coating. These films were pyrolysed intermediately at $\sim 150 °C$ for 2 min twice, and finally at 600 °C. The procedure followed for pyrolysis of PSZT films was the same as the one in the case of the PT seed layers. After coating the PSZT layer, the final crystallization was achieved by annealing the films at 650 °C, for 120 min in air. The metal/ferroelectric/metal (MFM) structure was formed by depositing gold top electrodes using cold D.C. sputtering unit (Model No. Desk II TSC) and a shadow mask ($\sim 500 \mu m$ in diameter). The thickness of the thin films was measured by using a surface profilometer (Model DEKTAK-3) after making a physical step by chemical etching using dilute HF/HCl solution. XRD patterns were recorded on a Philips thin film diffractometer (Model PW 3020) using a Cu(K_α) 1.54 Å X-ray in parallel beam geometry. The morphology of the films was characterized using atomic force microscopy (AFM, NT-MDT Solver P47H) in the resonant mode at 350 kHz and 38 nm amplitude. The dielectric constant (ε') and loss (tan δ) were measured at 100 kHz and at room temperature using an Impedence analyser (Agilent 4294A, precision impedence analyser). Hysteresis loops were recorded using an auto-matic P–E loop tracer (RT-66A) of Radiant Technologies. The remnant polarization (P_r) and coercive field (E_c) were obtained from the P–E hysteresis loop. C–V measurements were done using Agilent 4294A precision impedance analyser at 100 kHz with an oscillator level of 100 mV and a delay of 2 s during measurement. I–V measurements were done using Keithley 428 current amplifier along with SR 830 Lock-in-Amplifier.

3. Results and discussion

An X-ray diffractogram, showing patterns of a PSZT thin film is shown in Fig. 1. The XRD pattern shows the formation of a single-phase perovskite films. The XRD pattern of the films shows tetragonal behaviour at higher diffracting angles, however, this particular PZT having Zr/Ti ratio as 65/35 lie in the rhombohedral region of $PbTiO_3$–$PbZrO_3$ phase diagram [1]. It is reported that near morphotropic phase boundary (MPB), there could be a co-existence of both rhombohedral and tetragonal structure for lanthanum-substituted PZT [8]. The films were poly-crystalline in nature.

3.1. AFM measurements

The AFM micrographs are shown in Fig. 2(a)–(d). The average surface roughness (R_a) of the PZT films is shown in Table 1. It is evident from the surface morphology of the film (2% Sm:PSZT) on Pt/Si $\langle 1 0 0 \rangle$ substrate that there is an island formation which shows initial nucleation of the film but the same is not true for the films deposited on Pt/Si $\langle 1 1 1 \rangle$ substrate. This shows that there could be a preferential compositional dependence for the Pt/Si $\langle 1 0 0 \rangle$ substrate. It is also seen that as Sm (mol%)
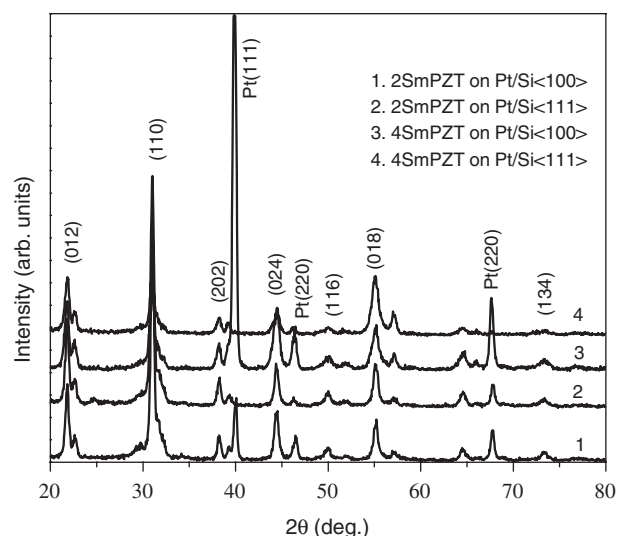
Fig. 1. X-ray diffractogram of Sm-substituted PZT thin films.
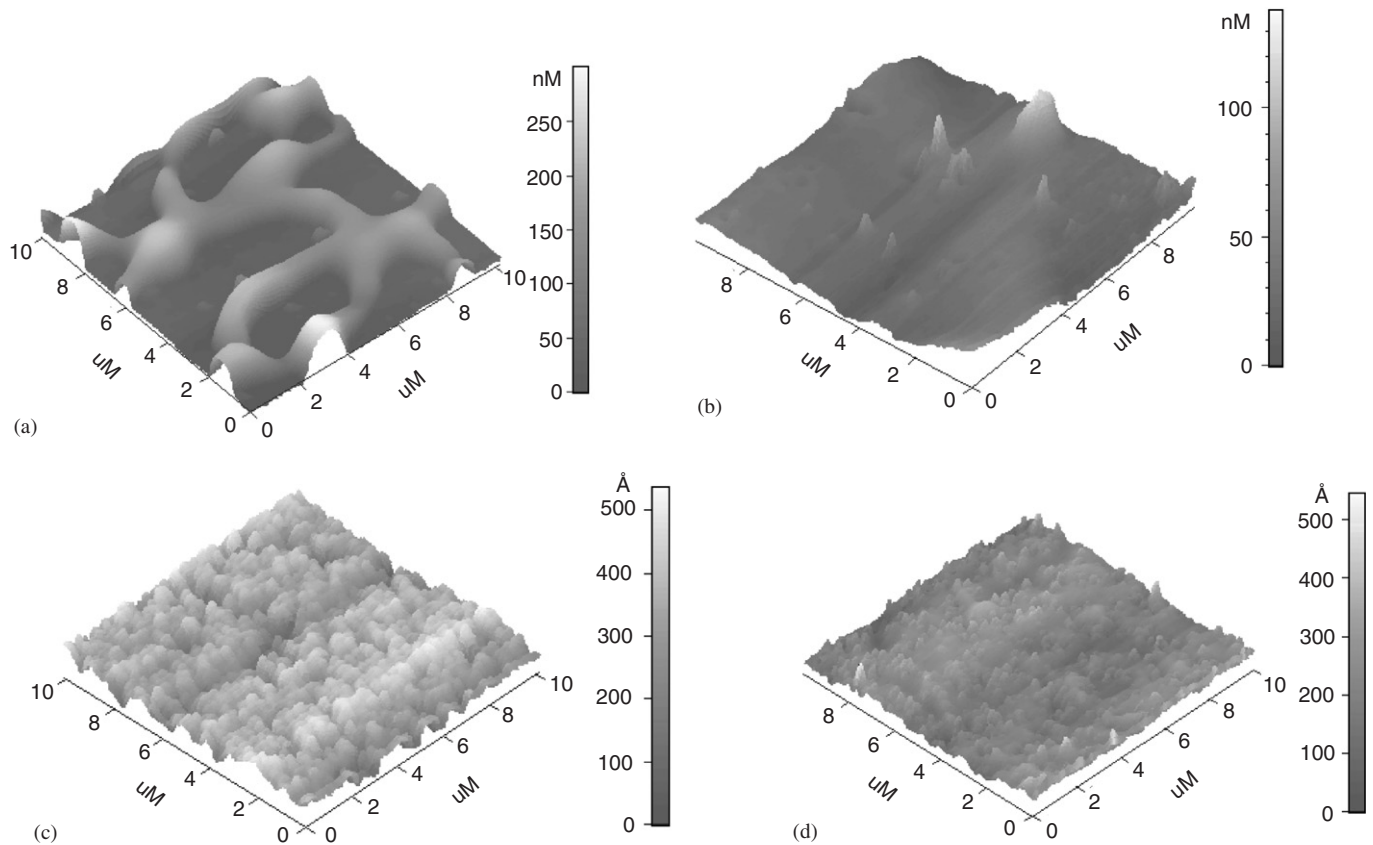
Fig. 2. Atomic force micrograph (3-D views) of (a) 2% Sm:PZT/Pt/Si ⟨1 0 0⟩, (b) 2% Sm:PZT/Pt/Si ⟨1 1 1⟩, (c) 4% Sm:PZT/Pt/Si ⟨1 0 0⟩ and (d) 4% Sm:PZT/Pt/Si ⟨1 1 1⟩.

Table 1
Capacitance, dielectric const, loss tangent (tan δ) and average surface roughness (R_a) of 2% and 4% substituted PZT thin films

Sample	Cp (nF)	tan δ	ε'	Average surface roughness (R_a) (nm)
2% Sm:PSZT on Pt/Si ⟨1 1 1⟩	1.38	0.183	477	7.69
2% Sm:PSZT on Pt/Si ⟨1 0 0⟩	3.53	0.369	1220	55.98
4% Sm:PSZT on Pt/Si ⟨1 1 1⟩	3.51	0.371	1213	4.47
4% Sm:PSZT on Pt/Si ⟨1 0 0⟩	3.37	0.423	1164	5.06

substitution in the PZT(65/35) is increased, there is a decrease in surface roughness of the films. It is to be noted that highly smooth surface ($R_a \sim 0.7$ nm for Pt/Si ⟨1 1 1⟩ and 3.83 nm for Pt/Si ⟨1 0 0⟩ substrates) films and 0.6 µm thickness have been obtained by authors for pure PZT (65/35) films [9].

3.2. I–V measurements

I–V curves for the PSZT films on various substrates are shown in Fig. 3. The shift in minimum of the I–V curve is evident for the films 3 (a–d). It is seen from the surface morphology of the films that there is an island formation/nucleation in the 2% Sm:PSZT film on Pt/Si ⟨1 0 0⟩ substrate. However, other films (3-b, 3-c and 3-d) are uniformly grown on the substrates and show similar shift in the minimum of I–V curve from $X = 0$. This kind of shifts

in the I–V curve of Sm/PZT films has not been reported earlier to the best of our knowledge. We have consistently observed these shift in Sm:PSZT films on Pt/Si ⟨1 1 1⟩ and Pt/Si ⟨1 0 0⟩ oriented substrates. The mixed behaviour of semi-conducting and ferroelectric characteristics of PZT dominate the conduction mechanism in these films which gives rise to shift in I–V characteristics to negative voltage side [10]. It is widely known that the ferroelectric film do give rise to space charge conduction mechanisms [11]. In order to avoid the shift in the minima of the curve, measurements were carried out from −5 to 0, 0 to +5 and −5 to +5 V. It was observed that all the films gave shifts when measurements were made from −5 to 0 V. The shifts in the voltage axis could be normally attributed to the formation of space charge region [11]. But here the shifts seem to be mainly due to Sm substitution since amount of shift voltage is quite high.
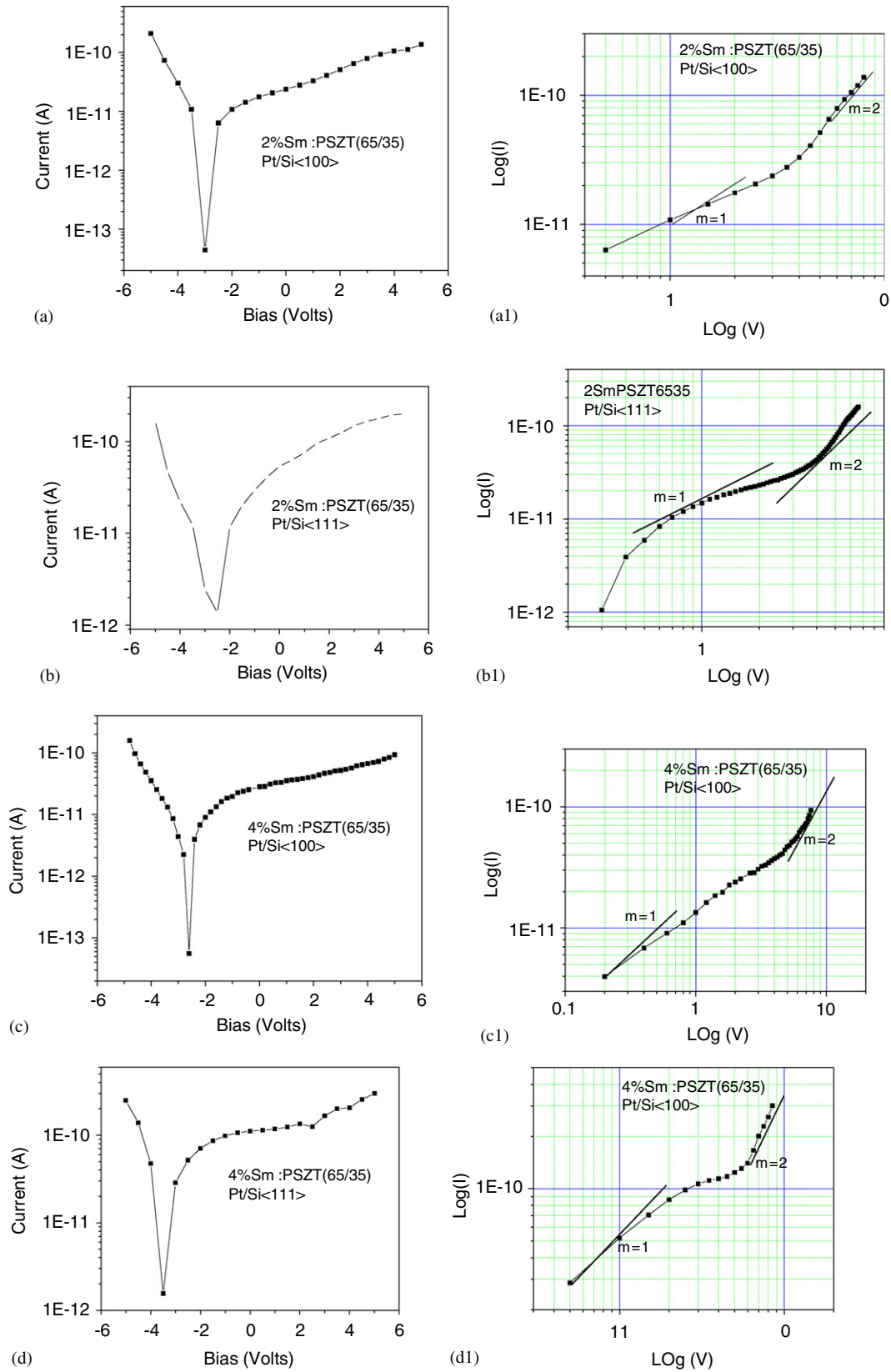
Fig. 3. *I–V* graph for Sm-substituted PZT (65/35) films: (a) 2% Sm:PZT/Pt/Si $\langle 1\,0\,0\rangle$, (a1) log *V* vs log *I* plot, (b) 2% Sm:PZT/Pt/Si $\langle 1\,1\,1\rangle$, (b1) log *V* vs log *I* plot, (c) 4% Sm:PZT/Pt/Si $\langle 1\,0\,0\rangle$, (c1) log *V* vs log *I* plot, (d) 4% Sm:PZT/Pt/Si $\langle 1\,1\,1\rangle$, (d1) log *V* vs log *I* plot.

In *I–V* characteristics of the Pt/PSZT/Au films (Fig. 3(a)–(d)), the forward bias represents the positive voltage applied on the gold electrode, whereas reverse bias corresponds to positive voltage across Pt electrode. The asymmetry observed in the *I–V* characteristics of the films is mainly due to work function difference of the electrodes. In general, four different regimes can be distinguished in the current–voltage (*I–V*) characteristics of low-conductivity materials. At low voltages the current density is proportional to the applied field (*ohmic regime*). At higher voltages the current density (*J*) increases as V^m ($m > 2$), which corresponds to trap-limited space charge limited currents (SCLC) followed by trap-filled limit and trap-free SCLC ($m = 2$). The trap limited space charge region can be clearly observed from the log–log plot of *I–V* of our films (Fig. 3(a1)–(d1)) with slope (*m*) being greater than 2. A shift of ∼3 V from $X = 0$ is also observed in the semi log curve of *I–V* characteristics (Fig. 3(a)–(d)). As such a kind of shift in voltage axis is not observed in case of Pt/PZT/Au films [9] this shift may be attributed to the presence of Sm in the A-site resulting in internal space charge field. As stated earlier, Sm^{3+} ions act as donor when it substitutes Pb^{2+} ion in the PZT lattice. These charges get accumulated near the gold electrode creating virtual internal field in the film [10]. This field gives rise to a noticeable high current even when no external bias is applied. The internal field created due to Sm substitution gets added to the positive bias and an increase in this current is observed. When reverse bias is applied across the film, the internal field compensates it and the current starts reducing to a minimum value at around −3 V. On increasing the reverse bias further, the current starts increasing again, resulting in a shift in voltage axis of *I–V* characteristics.

3.3. C–V measurements

The *C–V* curves for the films are shown in Fig. 4(a)–(d). The curve has the typical butterfly shape with two maxima. It is evident from the curves that the *C–V* hysteresis nature is less observed for the films deposited on Pt/Si ⟨111⟩ substrates as compared to Pt/Si ⟨100⟩ substrates showing a substrate effect. Further as the Sm (mol%) substitution is increased from 2% to 4% in PZT(65/35), there is increase in hysteresis in the *C–V* curve. This shows the compositional dependence behaviour of the PZT (65/35) with Sm^{3+} substitution causing internal field inside the film. It is also
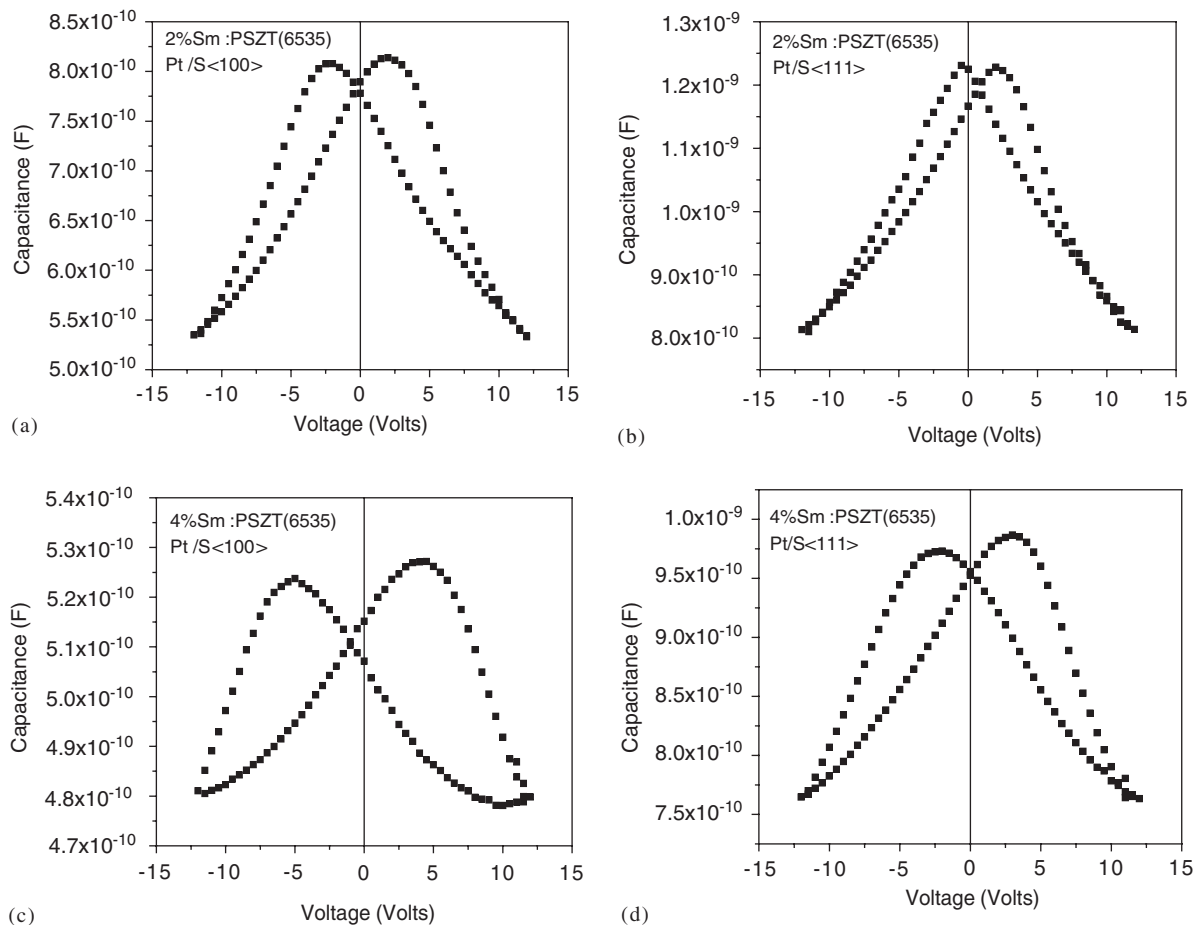
Fig. 4. Capacitance vs voltage curves for Sm-substituted PZT films: (a) 2% Sm:PZT/ Pt/Si ⟨100⟩, (b) 2% Sm;PZT/Pt/Si ⟨111⟩, (c) 4% Sm:PZT/Pt/Si ⟨100⟩ and (d) 4% Sm:PZT/Pt/Si ⟨111⟩.

observed that except for the curve in Fig. 4(d), all other curves show asymmetric behaviour at $X = 0$. This asymmetric behaviour may be attributed to the space charge regions, which could develop due to DC biasing in the C–V measurements [9] and also due to local internal field inside the sample [10].

3.4. P–E measurements

Fig. 5(a)–(e) shows polarization vs electric field hysteresis curves for the 2 and 4 mol% Sm-substituted PZT thin films. It is observed that as the applied field is increased the polarization increases and reaches to saturation at a substantial applied field. The values of remnant polarization ($+Pr$ and $-Pr$) as a function of applied voltage are plotted in graph 5(e). A maximum polarization ($P_r \sim 52\,\mu C/cm^2$) and corresponding coercive field ($E_c \sim 95\,kV/cm$) at 19 V was estimated from the P–E hysteresis curve for the 2% Sm-substituted PZT films grown on Pt/Si $\langle 1\,0\,0 \rangle$ substrates in this study. However, on Pt/Si $\langle 1\,1\,1 \rangle$ substrates there is a decrease in remnant polarization magnitude. A similar decrease in remnant polarization
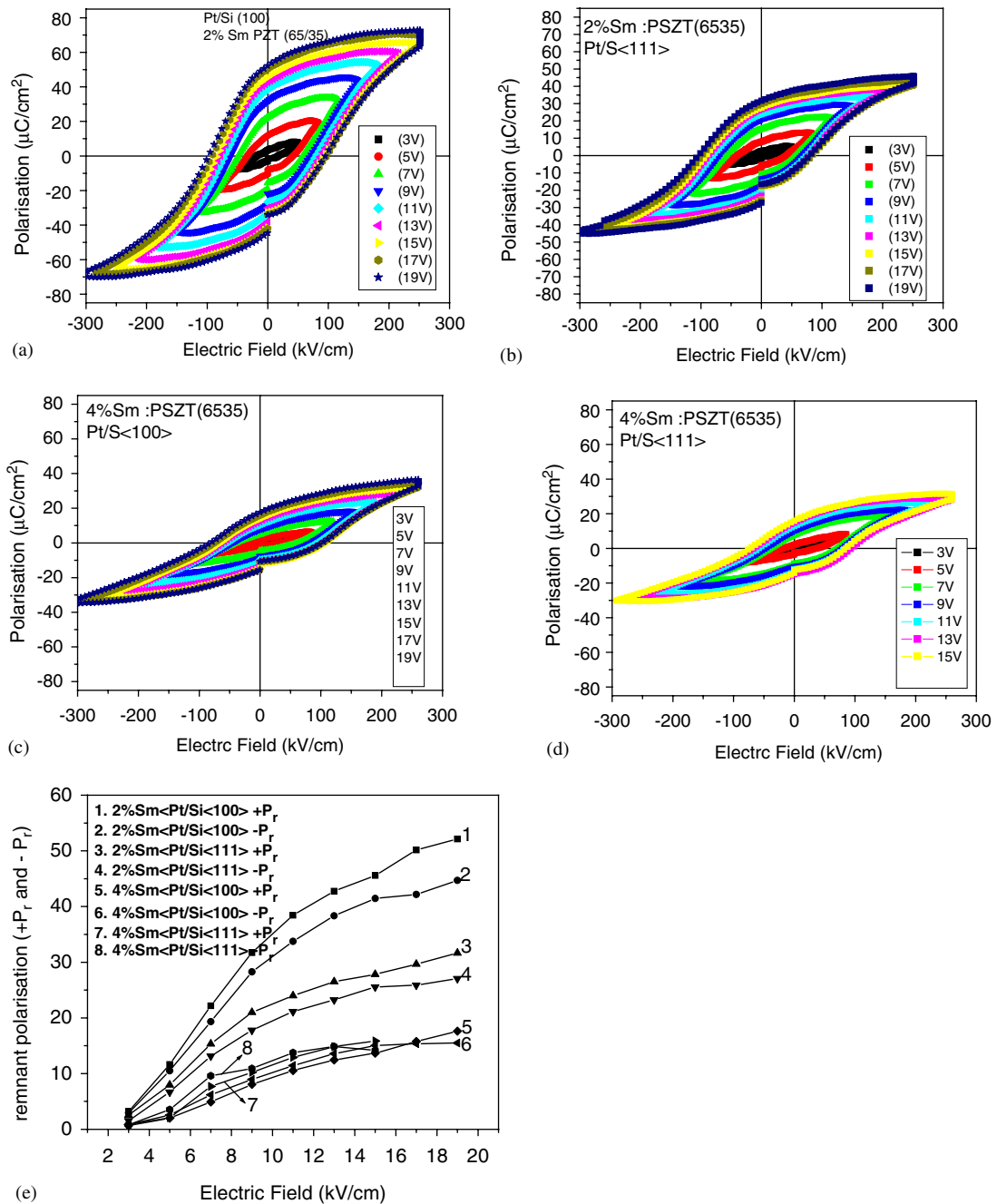
Fig. 5. Polarization vs electric field hysteresis loop for Sm-substituted PZT films: (a) 2% Sm:PZT/Pt/Si $\langle 1\,0\,0 \rangle$, (b) 2% Sm:PZT/Pt/Si $\langle 1\,1\,1 \rangle$, (c) 4% Sm:PZT/Pt/Si $\langle 1\,0\,0 \rangle$ and (d) 4% Sm:PZT/Pt/Si $\langle 1\,1\,1 \rangle$.
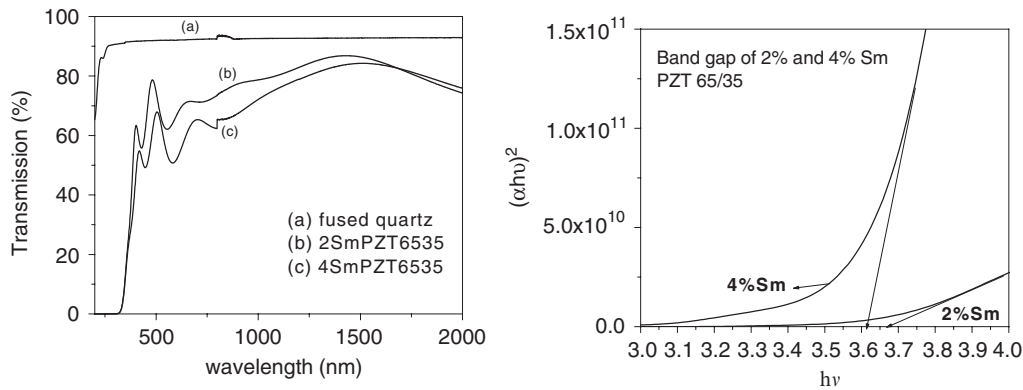
Fig. 6. Transmittance and band gap for Sm-substituted PZT thin films: (a) transmittance and (b) $(\alpha h\nu)^2$ vs $h\nu$ graph.

magnitude is also seen for the 4% Sm-substituted PZT thin films. This shows compositional and substrate orientation dependence behaviour for the Sm-substituted thin films. It is to be noted that authors have shown highest remnant polarization for the PZT (65/35) thin films [9]. From Fig. 4(e), it is observed that there is an asymmetry along polarization as well as field axes. The shift along the polarization axes in our case could be attributed to electrode asymmetry and due to formation of space charge region [11]. However, the asymmetry along field axis might be due to some internal bias which might be due to different electrode interfaces [12].

The dielectric constant (ε') and loss tangent $(\tan\delta)$ at room temperature and at 100 kHz is shown in Table 1. The value of dielectric constant for the films is much higher than that of reported PZT thin films [13]. A high dielectric constant here could be due to Sm^{3+} substitution in PZT. However, a stress in the films may affect the domain boundaries and possibly result in domain boundary motion [14,15].

3.5. Optical measurements

The transmittance curves for Sm-substituted films (2% and 4% Sm) deposited on fused quartz are shown in Fig. 6a. The variation in the interference pattern is due to the thickness and refractive index variation between the two films. It is also observed that transmittance decreases with Sm substitution in PZT. The optical absorption coefficient (α) has been calculated form the measured transmittance data and thickness of the film. In order to obtain the band gap of the film, $(\alpha h\nu)^2$ is plotted against the energy $(h\nu)$ as indicated in Fig. 6b. The intercept at the energy axis is the band gap energy of the material. The band gap of the 2 mol% Sm and 4 mol% Sm-substituted PZT films have been estimated as 3.67 eV and 3.61 eV $(\alpha = $ absorption coefficient, $h\nu = $ incident photon energy), respectively, which is in good agreement with the reported PZT thin films [16].

4. Conclusions

Single-phase PSZT thin films were deposited on platinized silicon ($\langle 100 \rangle$ and $\langle 111 \rangle$) and fused quartz substrates by sol–gel technique. Structural, electrical and optical properties have been studied and discussed. The AFM micrographs showed nano size surface roughness which smoothens further as Sm substitution in PZT is increased. The I–V study for the films showed shifts in current minima along the voltage axis. The reason for the above-mentioned shift is the internal field generated due to Sm substitution in PZT lattice. A reasonably high value of remnant polarization (Pr) was observed for the PSZT films. It was further observed that as the Sm substitution in PZT is increased, there is decrease in remnant polarization which shows compositional behaviour of the PZT thin films. The band gaps for the films are in good agreement with reported values.

References

[1] G.H. Heartling, J. Am. Ceram. Soc. 82 (1999) 797.
[2] C. Pramila, T.C. Goel, P.K.C. Pillai, Ferroelectrics 160 (1994) 157.
[3] C. Prakash, A. Bhalla, Ferroelectrics 262 (2001) 321.
[4] A.K. Tripathi, T.C. Goel, C. Prakash, Mater. Sci. Eng. B 96 (2002) 19.
[5] C. Prakash, O.P. Thakur, Mater. Lett. 57 (2003) 2310.
[6] S.R. Shanigrahi, F.E.H. Tay, K. Yao, R.N.P. Choudhary, J. Eur. Ceram. Soc. 24 (2004) 163.
[7] U. Chon, Ki-Bum, H.M. Jang, G-C. Yi, Appl. Phys. Lett. 79 (2001) 3137.
[8] V.M. Ischuk, V.N. Baumer, V.L. Sobolev, J. Phys.: Condens. Matter 17 (2005) L177.
[9] S.K. Pandey, A.R. James, C. Prakash, T.C. Goel, K. Zimik, Mater. Sci. Eng. B 112 (2004) 96.

[10] K. Abe, S. Komatsu, N. Yanase, K. Sano, T. Kawakubo, Jpn. J. Appl. Phys. Part 1 36 (1997) 5846.

[11] I. Boerasu, L. Pintilie, M. Pereira, M.I. Vasilevskiy, M.J.M. Gomes, J. Appl. Phys. 93 (2003) 4776.

[12] J. Lee, C.H. Choi, B.H. Park, T.W. Noah, J.K. Lee, Appl. Phys. Lett. 72 (1998) 3380.

[13] M. Tyunina, J. Levoska, A. Sternberg, S. Leppavuori, J. Appl. Phys. 84 (1998) 6800.

[14] B. Tuttle, T. Garino, J. Voight, T. Headley, D. Dimos, M. Eatough, in: O. Auciello, R. Waser (Eds.), Science and Technology of Electroceramic Thin Films, Kluwer Academic, Dordrecht, The Netherlands, 1995, p. 117.

[15] S. Ren, C. Lu, H.M. Shen, Y. Wang, Phys. Rev. B 55 (1997) 3485.

[16] X.G. Tang, A.L. Ding, Y. Ye, W.X. Chen, Thin Solid Films 423 (2003) 13.